



Development of die-less single-tool multi-point plate forming technology for 3D curved shape

Song Wu^{1,2} · Ninshu Ma^{1,2} · Sherif Rashed¹ · Naoki Osawa²

Received: 29 March 2021 / Accepted: 12 August 2021 / Published online: 1 September 2021
© The Author(s), under exclusive licence to Springer-Verlag London Ltd., part of Springer Nature 2021

Abstract

To avoid degradation of material properties, high equipment investment, low efficiency, and potential safety issues caused by conventional technologies like line heating, multi-point plate forming, and explosive forming, a new die-less single-tool multi-point plate forming (DS-MPF) technology is proposed. In DS-MPF, a moving bar is used as a single forming tool and combined with horizontal and vertical motions relative to the plate. To reduce forming force component from the membrane stress, simple support boundary condition is preferred to avoid the plate edge being bent, trimmed, or thinning after being formed. However, this boundary may easily cause instability of the forming process and worse geometric accuracy of a formed part if an unsuitable toolpath is employed. In this paper, the forming mechanism and toolpath design principle are clarified to develop this new technology. Numerical and experimental forming case from an 8-mm SS400 steel plate into a spherical surface with a radius of curvature of 1000 mm was performed to validate the new technology and its design principle. The strain analysis of results shows DS-MPF tends to be a local forming method. The formed plate normally has local positive bending strain at the tool-contacted area and limited negative bending strain at the tool-uncontacted area between adjacent strokes. Forming a 3D curved shape with high geometric accuracy in DS-MPF can be achieved with appropriate control of the local bending strain produced in each stroke, stroke position, and forming sequence.

Keywords Multi-point forming · SS400 · Spherical surface · DS-MPF · Die-less

1 Introduction

Three-dimensional (3D) curved thick plates are fabricated and used as components for the assembly of pressure vessels, fore and aft parts of ships, or other structures. For complex thick plate structures, there are two different forming strategies: first, manufacture each part and then assemble them; assemble flat plates of different shapes to approach the desired structure and then form the whole. The various conventional methods used today include line heating, cold bending, or multi-point

forming. These methods fall into the first category, and they are commonly employed and developed to form flat plates into different geometries and components of the desired three-dimensional shape. These components are then assembled into more complex structures. Explosive forming belongs to the second category. The acceptance and deployment of these techniques drop when more impact factors are involved, expensive tooling for different part geometries, low flexibility and efficiency of the manufacturing process, and the requirement for safety issues.

1.1 Line heating

In line heating, a heating source is utilized to heat the plate along designated lines. The heat cycle causes the plate to shrink and bend around the heating lines. Das and Biswas [1] summarized the categories of line heating processes based on the type of heat source: oxy-fuel gas flame, induction heating, and laser beam heating. In modeling line heating processes, researchers need to simplify and verify these heat input distributions. However, many variations, such as heating

✉ Song Wu
song.wu2022@outlook.com

✉ Ninshu Ma
ma.ninshu@jwri.osaka-u.ac.jp

¹ Joining and Welding Research Institute, Osaka University, 11-1 Mihogaoka, Osaka, Ibaraki 567-0047, Japan

² Department of Global Architecture Division of Naval Architecture and Ocean Engineering, Graduate School of Engineering, Suita, Osaka 565-0871, Japan

input distribution, residual stress and strain, material properties, and the skill level of workers, making accurate forming using this method seem difficult.

1.2 Multi-point forming (MPF)

Another widely used method is cold bending. In cold bending with uniform curvature, plates are formed using a pressing tool with a uniform curvature along a designed line. If a complex curved surface is to be formed by cold bending, multi tools and supports must be employed, which is called a multi-point forming technology. Li et al. [2] introduced a flexible manufacturing technique named multi-point forming (MPF). In this technique, upper and lower dies were replaced by a large number of elements (tools) with adjustable positions. Heo et al. [3] have conducted numerical analysis and a series of experiments for manufacturing of curved prototype using steel plate of 20 mm thickness. They also successfully developed the related software for process configuration and machine operation with automatic punch control for the above-mentioned method. In their experiment, two high-strength polyurethane sheets of 10 mm thickness were inserted between punches and plate to prevent surface defects and scratches on the punches and blank material. Wei et al. [4] introduced the idea of using multi-surface patch contact. A larger contact area between the square rams and the formed plate was obtained, which eliminated visible dimples, large local stress, and bending strain.

With the understanding of MPF and its forming mechanism, different variants of MPF were developed to improve the geometrical accuracy and surface quality of formed parts. Based on the theory of minimum plastic work, Cai and Li [5] presented a technique to adjust the relative positions of supports to shape a sheet metal along an optimum forming path to achieve the evenest deformation distribution in the final shape. Jia and Wang [6] investigated a new process of multi-point forming combining with individually controlled force-displacement (MPF-ICFD) and lots of rotational contact supports. They have successfully verified the feasibility of MPF-ICFD to reduce the spring back in the traditional multi-point forming (MPF). Dang et al. [7] presented a three-dimensional incremental bending method, which efficiently formed a $1000 \times 800 \times 5$ mm plate with errors less than 3 mm. They simplified a metal plate model as a shell and discretized it into a series of strips, each of which is modeled as a beam. In each incremental bending step, the deformation is relatively small, and hence, Euler–Bernoulli beam theory is applied to compute the bending of the strips. Li et al. [8] had discussed the effect of forming pins arrangement on the formed shape accuracy with sparse multi-point flexible (SMPF) tools. They concluded that increasing pins number in SMPF tools will decrease the profile errors and stress variations in the formed blank. However, the complexity and huge equipment investment of

the multi-tool and multi-support forming machine put serious limitations on this method. Die-less forming technologies such as incremental sheet forming (ISF) would be expected.

1.3 Incremental sheet forming (ISF)

As it is known that ISF, as a die-less method, is characteristic of employing a simple, cheap bar as a forming tool and avoid large investments on die. In the ISF process, a forming tool tip slides or rolls over a metal sheet to incrementally form it into the required geometry. Silva et al. [9] found that, with fixed boundary conditions and a hemispherical tool, the material contacted with the tool exhibits a plane strain state in the contact region. Due to the fixed boundary, sheets suffer large meridional stress and thickness reduction along an inclined wall. For jig-fixed sheet edges, later trimming is required after the ISF process, and it will increase material costs and man-hours. Young and Jeswiet [10] employed a COS law of wall angle in Eq. (1) to predict the final thickness of a target shape. The maximum wall angle is generally regarded as an index to evaluate and control the formability of different materials.

$$t_1 = t_0 \times \cos\alpha \quad (1)$$

where t_1 and t_0 are the final and initial thicknesses of a sheet and α is the wall angle. With a large reduction in thickness, the membrane strain $\varepsilon_{\text{membrane}}$ along the inclined wall is the main component of total strain ε in Eq. (2). It is because the bending strain $\varepsilon_{\text{bending}}$ between the upper surface and the lower surface of the inclined wall is relatively smaller in thin sheet, especially for a straight inclined wall.

$$\varepsilon = \varepsilon_{\text{membrane}} + \varepsilon_{\text{bending}} \quad (2)$$

Behera et al. [11] concluded that, due to the local forming nature, the forming force with small tools (10–20 mm) is small. Therefore, the forming force can be afforded by three different kinds of equipment, CNC milling machines, robotic arms, and specially adapted equipment. However, as friction or rolling resistance applies a lateral force on the tool, the need to keep this lateral force small restricts the formed sheet thickness. In addition, the particularly long manufacturing period also further reduces the efficiency of the forming process.

1.4 Explosive forming

Zhang et al. [12] proposed a highly efficient die-less forming technique called explosive forming that can improve forming forces and decrease forming periods. As illustrated in Fig. 1, the authors presented the manufacturing procedure of this method for a spherical tank. This technology works by the explosion of explosive material inside a semi-spherical

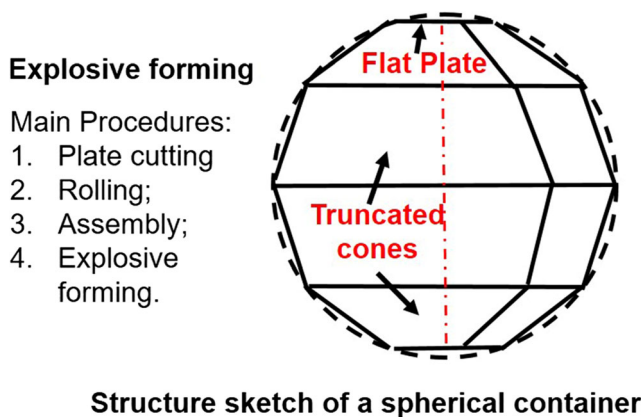


Fig. 1 Structure sketch of the container with die-less explosive forming

structure to transform it into a complete sphere. Initially, some truncated cones were produced by a rolling machine and then welded together to yield the so-called four cones vessel structure. Afterward, the two upper and lower parts were covered using a flat round plate with a hole at its center. The tank was filled with water to homogenize the explosive shock. Zhang et al. [13] continued to investigate structure design for die-less explosive forming of spherical vessels by comparing three-, four-, and five-cone structures. The five-cone structure could be expanded into a spherical shape perfectly due to minimal strain distributions around the welded regions. Except for the shape design, Mehrasa [14] analyzed the amount of explosive needed for this process in terms of the vessel's diameter and thickness. However, several issues, such as long and complex forming procedures, the strength of the weld region after an explosion, and safety problems while dealing with the explosion, may influence the application of explosive forming.

1.5 A novel thick plate forming method DS-MPF

To form a plate more efficiently, safely, and economically, a new plate forming technology DS-MPF is proposed. This method is an alternative to ISF method, especially for plates of thicknesses that cannot be formed by ISF. Unlike MPF and SMPF, DS-MPF is a die-less method, and it only needs one pressing tool and several simplified supports perpendicular to the plate near the boundary. As compared to explosive forming, this method is more efficient and safer due to the removal of parts of the procedures, as well as the absence of explosives.

In Fig. 2a, the tool does not slide or roll on the plate to avoid tool failure due to excessive lateral force, also to avoid scratching the plate surface. The tool head has three degrees of freedom in three directions; it moves along the X-Y-Z direction with respect to the plate being formed and its supports. In each stroke, the tool moves down vertically to press the plate (leaving a toolpath mark) and returns vertically up to its original position and then moves horizontally in the X-Y plane to

be positioned for the next stroke. In this way, the plate is formed in successive strokes in which lateral force is limited. As in other cold forming processes, issues with spring back and surface quality (smoothness) still occur in DS-MPF. In thick plate forming, to bring down total forming force by reducing the membrane strain $\varepsilon_{membrane}$, the use of simple support boundary is preferred. Without obvious membrane strain $\varepsilon_{membrane}$ in Eq. (2), bent plate has a limited thickness reduction and needs a small forming force; thus, its bending strain may account for the main part of the total strain in DS-MPF. The DS-MPF can also be used to form the container in Fig. 1. In Fig. 2b, a new structure sketch of the container was drawn according to the concept of DS-MPF. This structure consists of several sub-components with the same curvature and different edges. With the same curvature, the type C spherical component can be trimmed into type D and vice versa. For C-type components, the edge shape required for accurate assembly can be acquired by cutting in advance on the initial flat surface, or through trimming after forming in DS-MPF.

Fig. 3 shows the workflow to form a sub-component in DS-MPF, including CAD, CAM, and forming machine. In this paper, the forming mechanism of DS-MF and its detailed procedures will be investigated and discussed in the forming of a spherical sub-component with a specific radius of curvature.

2 Theoretical design of DS-MPF

In this section, the characteristics of this new thick plate forming method will be investigated, including the forming mechanism of DS-MPF, the boundary condition, the number of strokes, stroke position, and forming sequence.

2.1 The forming mechanism of DS-MPF: local bending

For part by formed DS-MPF, its cross section profile consists of slightly bent arc segments (tool-contacted area) and gradually curved connection areas (uncontacted area with larger local curvature radius). For the tool-contacted area marked with point Q in Fig. 4a, the formed local curvature radius \bar{r} has a negative relationship with the deflection at the periphery area of the tool. As the formed line is bent more severely, the local curvature radius \bar{r} and the deflection Z_{max} may change from \bar{r}_C and Z_{Cmax} to its target \bar{r}_A and Z_{Amax} . For achieving a smooth curve and saving more manufacturing time, an intermediate state with an allowable deviation is acceptable, which corresponds to the required line B with Z_{Bmax} and \bar{r}_B . The total strain along X direction ε_x can also be separated into two components, involving strain for compression or tension component $\varepsilon_{x\ membrane}$ and strain for bending component $\varepsilon_{x\ bending}$ (see Eq. (2)). In DS-MPF, $\varepsilon_{x\ membrane}$ is limited due to simple support boundary, and it will not influence the bending of

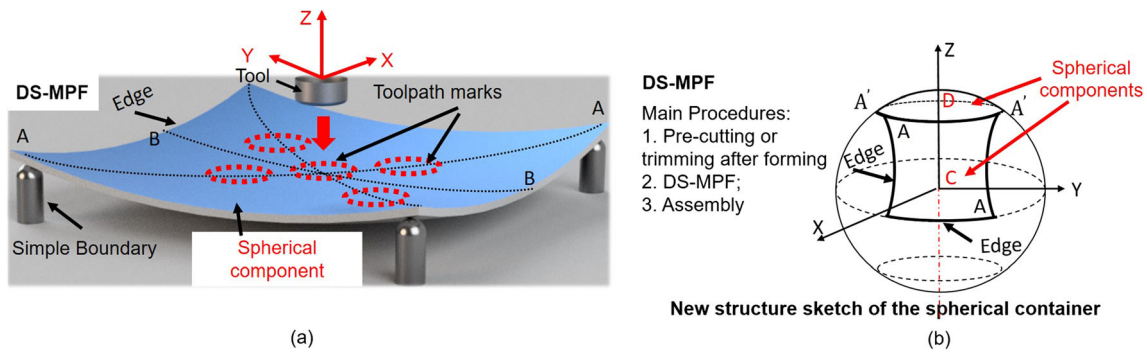


Fig. 2 (a) The novel plate forming technology DS-MPF and (b) new structure sketch of the container in Fig. 1

plate. In Fig. 4b, the bending strain $\Delta\varepsilon_{x\ bending}$ is used to quantify the strain difference between an upper surface strain $\varepsilon_{x\ upper}$ and a lower surface strain $\varepsilon_{x\ lower}$ (see Eq. (3)). Since different local radii of curvature correspond to various types of bending strain, the overall formed radius of curvature depends on the combination of those local radii of curvature in the area of each stroke. Thus, controlling bending strain at each stroke and their distribution can decide the local radius of curvature and its deflection at each point; further, determine the overall radii of curvature and profile error. Normally in DS-MPF forming, the calculated elastic strain is limited as compared to the plastic strain.

$$\Delta\varepsilon_{x\ bending} = \varepsilon_{x\ lower} - \varepsilon_{x\ upper} \tag{3}$$

2.2 Target spherical case formed with 8 mm SS400 steel thick plate

Through forming a spherical case featured with a radius of curvature \bar{R}_{Target} equal to 1000 mm, plotted in Fig. 5, boundary condition and toolpath design principle in DS-MPF will be clarified in the following subsections. Curves AC, BD, EF, and GH are two-dimensional curves on this surface. The

maximum depth is 56.80 mm at the center. Initial experiment samples are $500 \times 500 \times 8$ mm plates, made of SS400 steel, which is popular steel in the construction of bridges and ships.

\bar{R} is the overall radius of curvature of the formed profile along each section, calculated from three points on the section (such as the three points G and H and the central point along curve GH in Fig. 5).

To evaluate the overall and local geometric accuracy, two error definitions were used: the radius of curvature \bar{R} with its relative error δ as in Eq. (4) and the local maximum geometric deviation ΔH , deviated from the target.

$$\delta = \left(\bar{R} - \bar{R}_{Target} \right) / \bar{R}_{Target} \times 100\% \tag{4}$$

2.3 Boundary condition and number of strokes

DS-MPF is a multi-point forming. The term “multi-point” refers to not only multi-strokes but also multi-supports along plate edges. Spherical shape in Fig. 5 with \bar{R}_{Target} and thickness t may be formed with 8 supports under the plate. In Fig. 6, strokes will be positioned along those section lines like sections A-A and B-B. Every two supports are positioned on sections A-A or B-B with a distance of $2f$ or $2e$. Meanwhile, for achieving a smaller deviation, a small angle of φ is required to reduce the deviation in the areas between adjacent sections. For reducing related factors discussed in this paper, φ was set to a fixed value of 45° . The supports C and D were positioned along the cross sections A-A and B-B. The initial plate was only supported by support C. Since the absence of the fixed boundary and extremely simplified support condition, a slight rotation of the plate around the center occurred in the forming process. A flat support D with surface contact was preferred as compared to support C with point contact. The point contact between the plate and support C will result in localized unevenness in the middle of plate edge. Multiple closely aligned supports C can also be employed as an alternative to support D. The distance between the initial plate surface and flat support D was defined as Δh , which is affected by the target shape and spring back quantity.

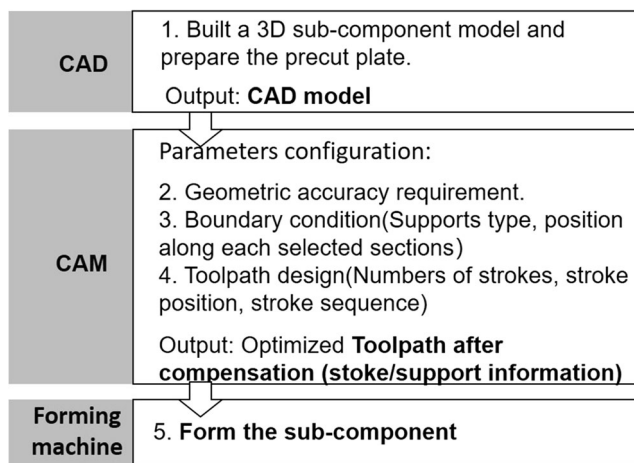
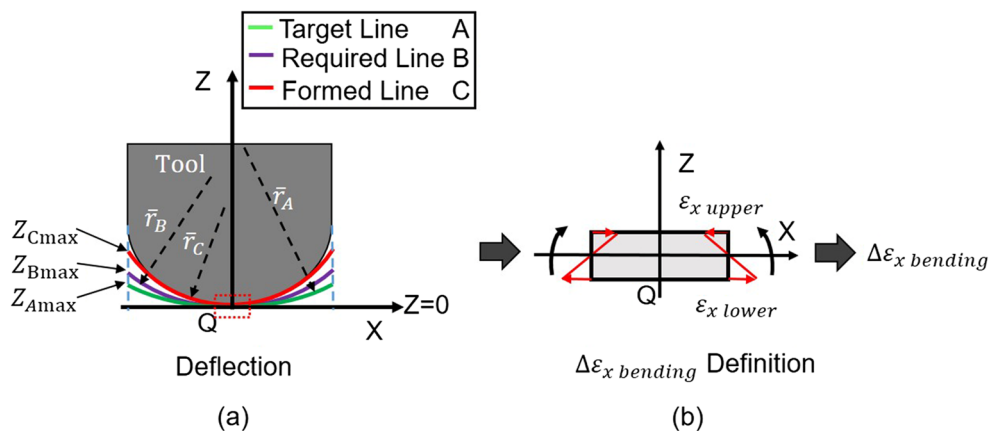


Fig. 3 Work flow in DS-MPF

Fig. 4 (a) Local plate bent with the different deflections and local radii of curvature at point Q. (b) The definition of bending strain



The process of forming a two-dimensional curve OQP colored in green, with a target radius of curvature \bar{R}_{Target} and a radial angle θ_0 in Fig. 7a, was used to explain the basic toolpath design strategy along each cross section. The tool radius of curvature is \bar{R}_{tool} . Each arc sub-segments (OQP=2OQ=4NQ=8LQ) corresponds to different angles θ_i ($i = 0, 1, 2, 3, \dots$). A straight beam supported at endpoints O and P is to be bent by the tool into the arc segment OQP. Ignoring spring back, if only one stroke is adopted, the minimum deviation can be achieved by placing the stroke at Q in the middle of OQP. The beam parts OQ and QP remained almost straight. ΔH_0 is the initial maximum deviation in the central area. ΔH_1 is the deviation between OQ and target segment ONQ. With a second stroke at the middle point N of arc segment ONQ, the deviation rapidly decreases to ΔH_2 . The deviation ΔH_i is decided with θ_i and \bar{R}_{Target} (see Eq. (5)). The R is the radial distance of the second stroke, calculated in Eq. (6). The radial distance between real contact position and the axis was defined as R_c (see Eq. (7)). After the first stroke in the center, parameters R or R_c for the distance of the next stroke are used to control the geometric accuracy. Fig. 7b presents the relationship between numbers of strokes (θ_i , ΔH_i , R) and the ratio of θ_i/θ_0 , while $\theta_0 = 38.8^\circ$ and $\bar{R}_{Target} = 1000\text{ mm}$ ($OP = 664\text{ mm}$). Along the cross section, as θ_i/θ_0 decreases proportionally, the number of strokes will increase leading to a rapid decrease in ΔH_i . When ΔH_i is selected as 3.6 mm, accordingly, the number of strokes is 3 and R is equal to 163 mm. The deviation caused by spring back will be corrected by using a toolpath (strokes sizes) compensating method.

$$\Delta H_i = \bar{R}_{Target} \cdot (1 - \cos\theta_i) \tag{5}$$

$$R = (\bar{R}_{Target} - \bar{R}_{tool}) \cdot \sin\theta_i \tag{6}$$

$$R_c = \bar{R}_{Target} \cdot \sin\theta_i \tag{7}$$

When thickness t and \bar{R}_{Target} of the formed plate are 8 mm and 1000 mm, respectively, the predicted $\Delta \epsilon_{x\ bending}$ of the target shape is 0.008 (see Eq. (8)). If tool radius \bar{R}_{tool} is set to be 100 mm, the predicted $\Delta \epsilon_{x\ bending}$ in pure bending case is about 0.077.

$$\Delta \epsilon_{x\ bending} = \epsilon_{x\ lower} - \epsilon_{x\ upper} = \ln \left[\frac{(\bar{R}_{Target} + t)}{\bar{R}_{Target}} \right] \tag{8}$$

2.4 Finite element modeling

To associate the actual stroke position with deviation in DS-MPF of the spherical surface, the relationship between R and ΔH needs to be calibrated through numerical modeling in commercial software Ls-Dyna. The finite element model (flat plate with $500 \times$

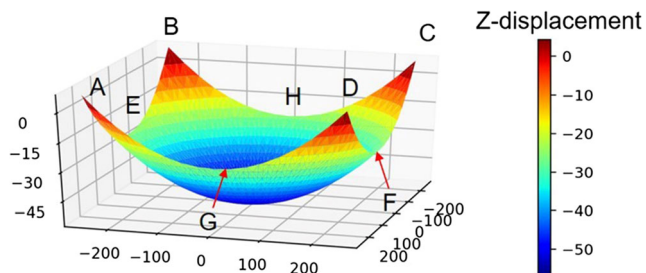


Fig. 5 Spherical surface target with a radius of 1000 mm

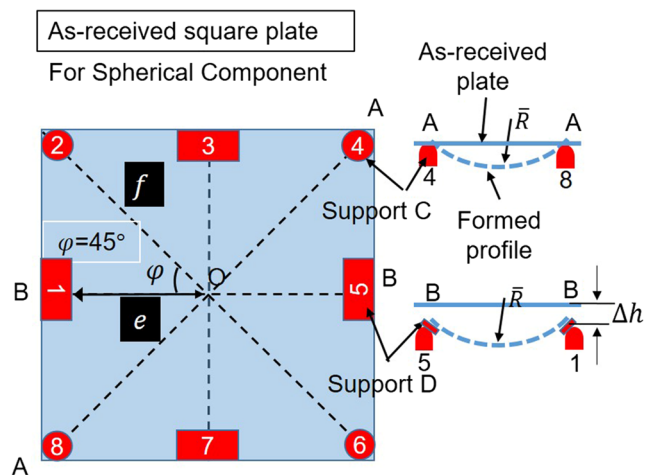


Fig. 6 Numbers of supports and their position for spherical surfaces in DS-MPF

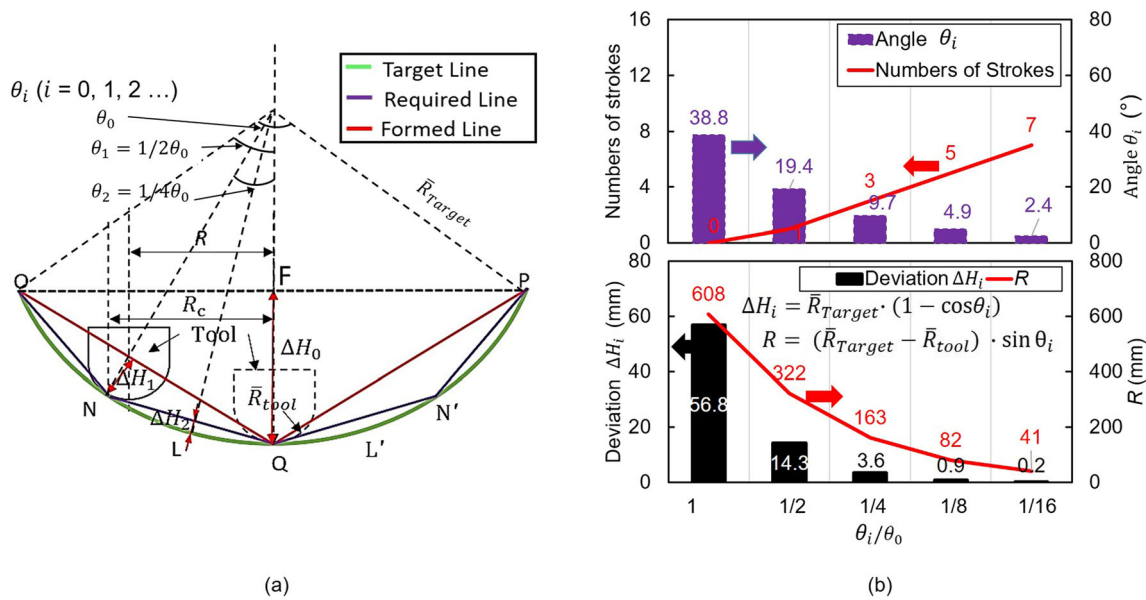


Fig. 7 (a) Tool strokes for a 2D curve target and (b) the relationship between numbers of strokes, angle θ_i ($i = 0, 1, 2 \dots$), deviation ΔH_i , radial distance R , and the ratio of θ_i/θ_0 , while $\theta_0 = 38.8^\circ$ ($OP = 664$ mm) and $R_{target} = 1000$ mm

500 × 8 mm) used in the analysis is shown in Fig. 8. Selectively reduced integrated solid element was selected as the solid element formulation. The model was designed with solid elements 5 × 5 × 1 mm. An elastic-plastic material type 24 (MAT PIECEWISE LINEAR PLASTICITY) with stress versus effective plastic strain curve was defined in Ls-Dyna. The tool was defined as a rigid body with a diameter of D60 mm and tooltip radius R_{tool} of 100 mm. The diameter of supports at the corners (supports C) is 30 mm, and the radius of their tips is 125 mm. The contact type between support C and the initial plate is point contact. These flat supports D (50 × 100 mm) were positioned at the middle of each edge to provide sufficient surface contact between plate and support.

The physical and mechanical properties of 8-mm thickness SS400 plate are listed in Table 1, including E (Young modulus), TS (tensile stress), and YS (yield stress). The used tensile test specimen of SS400 is shown in Fig. 9a. The resulting true stress-strain curve and hardening curve can be seen in Fig. 9b. The true stress-strain curve was fitted with the red curve using Eq. (9).

$$\sigma_t = 715 \cdot (0.018 + \epsilon_t^p)^{0.165} \tag{9}$$

2.5 Stroke position

In Fig. 10a, three strokes along each section B-B were applied to form a spherical shape, 1st point stroke in the center, additional 4 strokes on the 1st loop with a distance of R away from the center. After the strokes on the 1st loop, the corresponding nonlinear fitting Eq. (10) was used to derive the relationship between R and the maximum local profile error ΔH along this section. Parameters a, b, c, and d can be decided by the radius of curvature of the target and tool geometry. The effect of the allowable distance R on the formed profile was presented in Fig. 10b. The parameters a, b, c, and d can be acquired from the simulated results of cases with different R . When R changed from 35 to 75 mm and then to 118 mm, the maximum geometric error rose from 2.46 to 3.25 mm and finally to 4.56 mm. In this case, parameters a, b, c, and d were separately equal to 5.564×10^{-2} , 8.621×10^{-2} , -7.475×10^{-4} , and 2.806×10^{-06} (see Eq. (11)). For a product with thick plate like in ship manufacturing industry, the

Fig. 8 Finite model

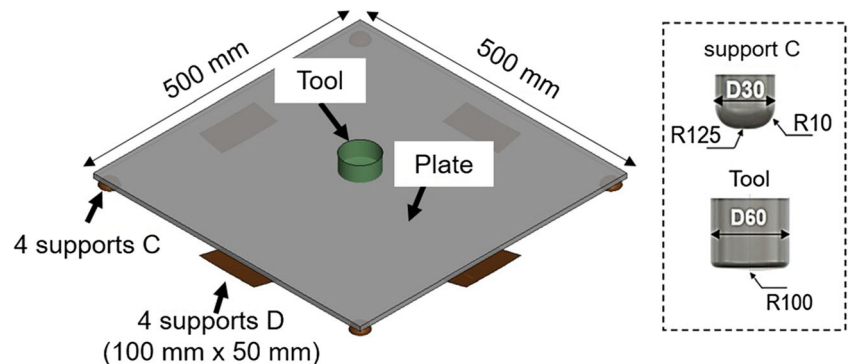


Table 1 Physical and mechanical properties of the 8-mm thickness SS400 plate in tensile test

| Material | E (MPa) | Poisson's ratio | TS (MPa) | YS (MPa) | Elongation (%) |
|----------|---------|-----------------|----------|----------|----------------|
| SS400 | 203369 | 0.3 | 450 | 369 | 24 |

required geometric accuracy is not too high. If setting the allowable profile error below 4.00 mm, according to Eq. (11), the maximum R should be smaller than 100 mm, as shown in Fig. 10c.

$$\Delta H = a + bR + cR^2 + dR^3 \tag{10}$$

$$\Delta H = 5.564 \times 10^{-2} + 8.621 \times 10^{-02}R + -7.475 \times 10^{-4}R^2 + 2.806 \times 10^{-06}R^3 \tag{11}$$

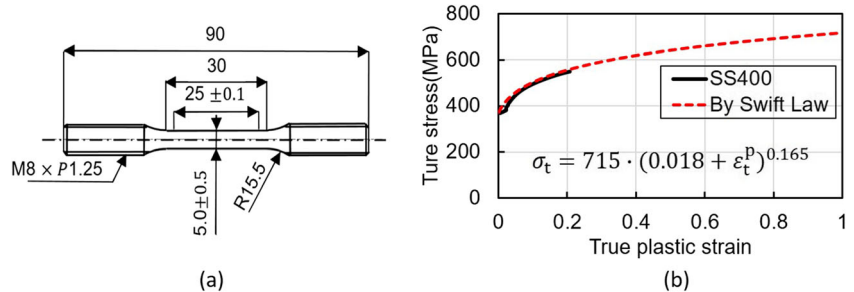
A 9-point toolpath 1 starting from the center in Fig.10 was used to verify the correctness of the prediction error of Eq. (11). Eight strokes in the outer area were located with distances of R118 mm and R167 mm, respectively, along sections A-A and B-B. For toolpath 1, each stroke equals Z-displacement of the tool from the initial plane ($Z = 0$ mm) to the position tangent to the spherical surface in Fig. 4. For the central stroke, the Z-displacement of the tool was set to be -56.8 mm.

Fig. 11 displays profile comparison between formed part by toolpath 1 and its target. The resulted \bar{R} along sections A-A and B-B were 978 mm and 1062 mm, respectively, close to the target. For A-A, the maximum deviation was 6.7 mm; for B-B, the maximum deviation was 4.5 mm. These local deviations were a bit higher than the theoretical deviation of 3.6 mm in Fig. 7b. As R decreased from 167 to 118 mm, the maximum deviation dropped from 6.7 to 4.5 mm. The maximum errors of 6.7 mm and 4.5 mm equal the predicted values 6.7 mm and 4.4 mm by using Eq. (11).

2.6 Forming sequence

As there are many combinations of strokes to form a trajectory, two basic forming sequences, from inside to outside (IN/OUT) and from outside to inside (OUT/IN), were mainly discussed.

Fig. 9 (a) SS400 tensile test specimen, and (b) true stress-strain curve.

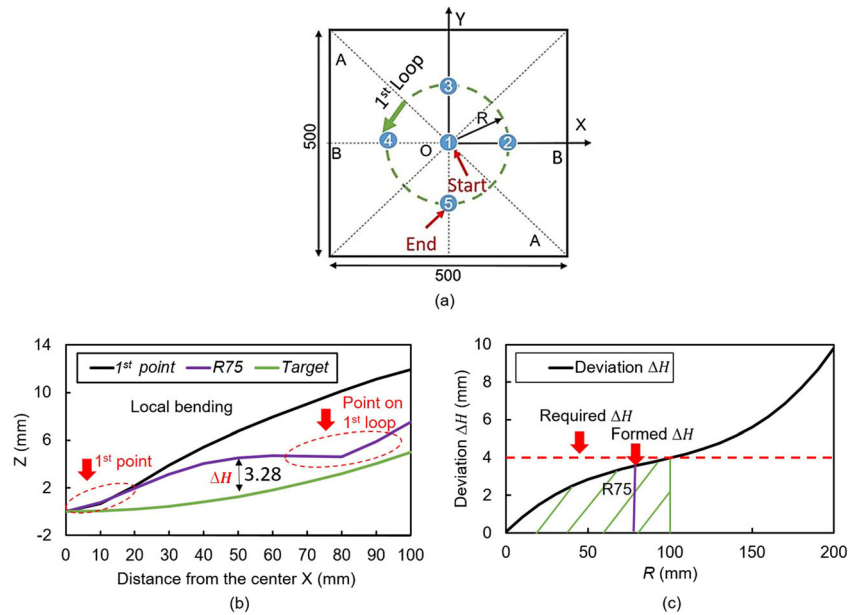


The effect of the forming sequence on Z-displacement histories of formed parts was investigated. In comparison to toolpath 1, toolpath 2 has the same stroke and opposite forming sequence; Fig. 12 a, b, c, and d and display formed parts with toolpath 1 and toolpath 2. The Z directional displacement contour of toolpath 1 was rather square, while the displacement contour of toolpath 2 was close to circular. This suggests that additional stroke points are needed to obtain a circular contour for the part formed by toolpath 1. The edge profile comparison between toolpath 1 and toolpath 2 in Fig. 12c and Fig. 12d illustrates that the shape formed by the OUT/IN toolpath requires additional support to obtain an accurate edge profile. The maximum Z-displacement of the part by IN/OUT toolpath 1 was 57.55 mm, closer to the target value of 56.8 mm than that formed by the OUT/IN toolpath. Five points, including points 1 (at center) and 6-9 (in the outer area with R equal to 167 mm), were selected to record the Z-displacement history during each stroke (see Fig. 12e and f). In Fig. 12e, when the tool contacted the plate at point 1, the central area had a large displacement than the outer area. The spring back quantity was similar for both areas. In forming process, the spring back quantity tends to decline due to the reducing Z-displacement for each stroke. When the tool pressed at point 6, areas belonging to the other 4 points had a smaller Z-displacement in the forming process. When this toolpath was finished, Z-displacement of points 6-9 were all close to -37.6 mm. In Fig. 12f, the outer loop areas from point 6 to point 9 had different Z-displacements, varying from -44.7 to -48.8 mm. It indicates the IN/OUT toolpath can lead to higher stiffness in the center, improve forming stability of the forming process, and achieve better geometric accuracy.

3 Experiment

To validate the feasibility of this technology and to confirm good agreement between experimental and simulation results, the corresponding experiment and simulation with an optimized toolpath will be conducted. The experimental setup (fixtures, tool, plate, the press machine) and the optimized toolpath are explained in this section.

Fig. 10 (a) Stroke position; (b) profile comparison between the formed plate and the target after finishing the strokes on the 1st loop with different R from 35 mm to 118 mm; (c) process window of parameter R



3.1 Experiment setup

The DS-MPF experiment was conducted using a 2000 kN-class AC servo press (model H1F200; Komatsu Industries) in Fig. 13a. The designed tool and jig are shown in Fig. 13b. A top view and a sectional view of the fixture were given in Fig. 13c and d. The pressing tool was manufactured from high carbon steel with a diameter of 60 mm and a tooltip radius of 100 mm. It was then hardened to minimize its deformation during the experiment. The entire supporting jig has the size of 600 × 600 mm. The tool is free to move in a space of 400 × 400 mm. The jig includes a frame composed of two plates 600

× 600 × 16 mm, tied together with 8 supports E. Supports E with bolts served to support the plate in the horizontal directions. Only 4 lower supports C and 4 supports D were fixed to the frame with threads and nuts to provide adjustable height supports for the formed plate. Considering the influence of spring back compensation, the relative height of supports D will be adjusted to positions lower than the target surface.

3.2 Toolpath design

To further verify the design principle and investigate the mechanism of DS-MPF, 33 strokes in toolpath 3 (see Fig.

Fig. 11 a The schematic diagram of toolpath 1. Profile comparison between the simulated result with toolpath 1 and target along sections (b) A-A and (c) B-B

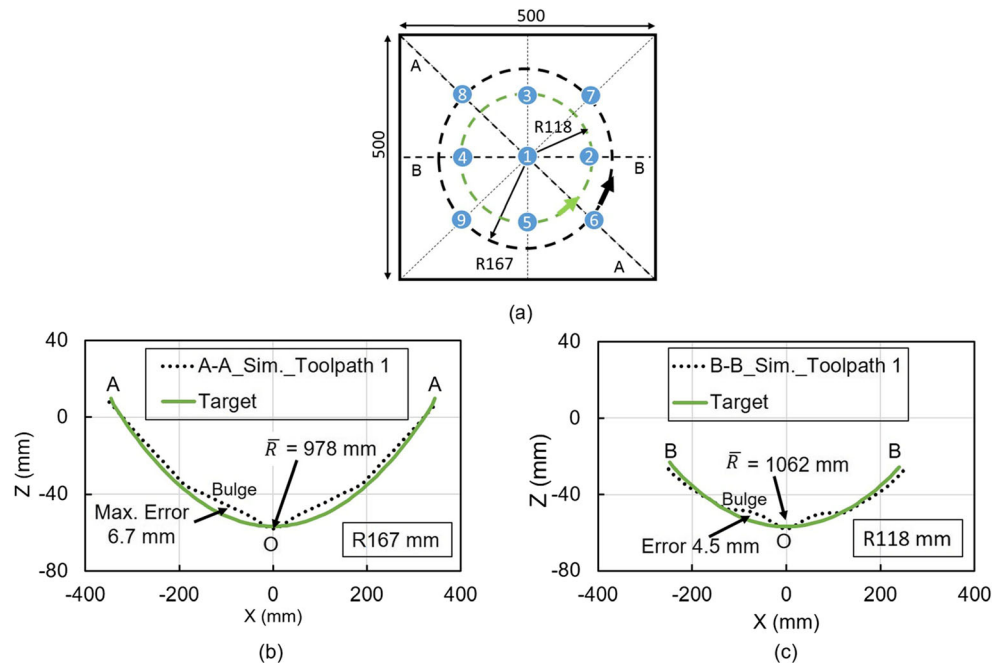
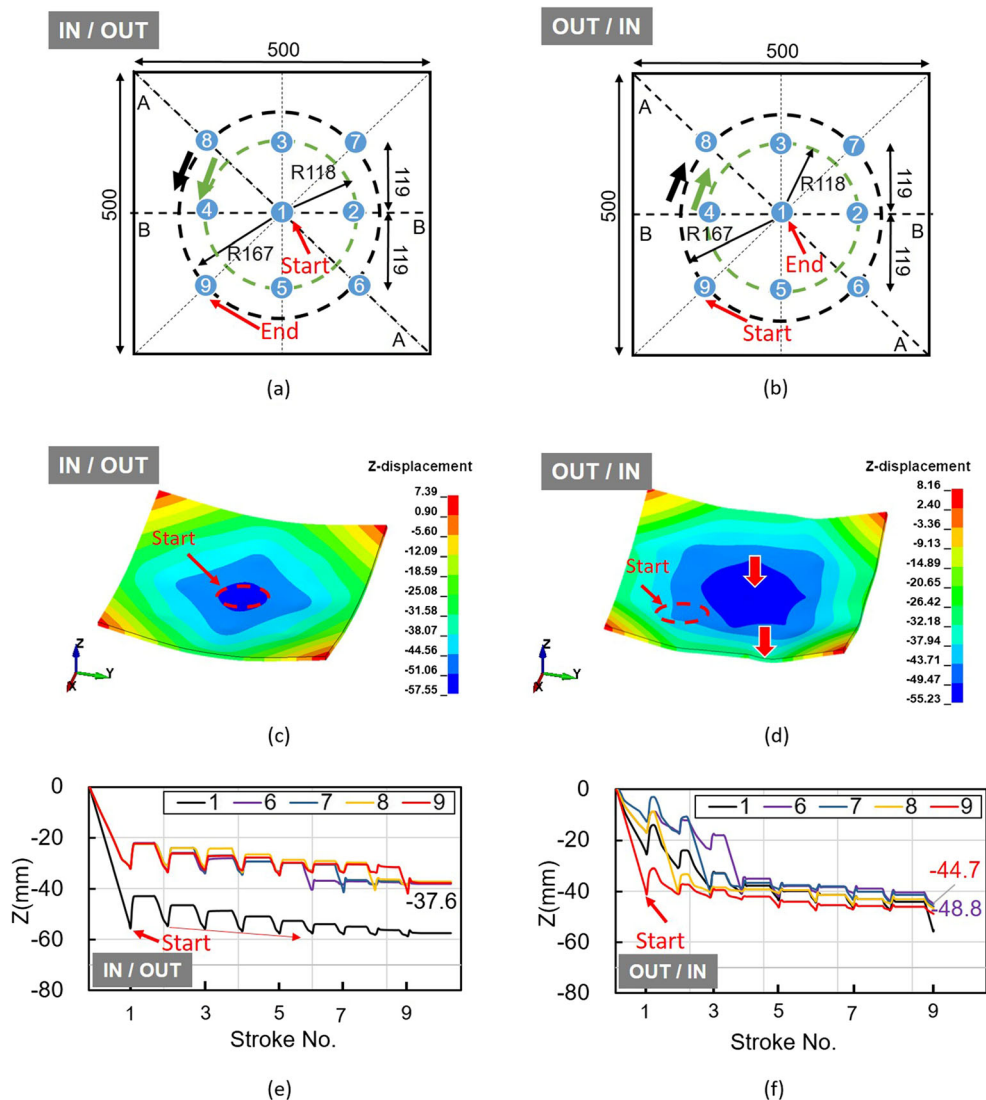


Fig. 12 (a) Toolpath 1(IN/OUT) and (b) toolpath 2(OUT/IN) with 9 strokes. Simulated contours by (c) toolpath 1 and (d) toolpath 2. Z-displacement histories of points nNo. 1 and, 6–9 with (e) toolpath 1 and (f) toolpath 2



14a) and their Z-displacements after compensation (see Fig. 14b) were designed for the target shape in Fig. 5. In Fig. 14a, all strokes were put along 4 selected straight lines passing through opposite corners and mid-points of opposite edges. In Fig. 14b, the initial Z-displacement of each stroke (before compensation) at location X, Y was taken as the Z-displacement which made the tool profile tangent to the target surface. Compensation iterations method (see Appendix) for spring back was applied to each stroke to acquire toolpath 3 and achieve higher geometric accuracy.

As it is known that overall curvature may influence the assembly accuracy of formed plates, local geometric deviation will affect the smoothness of the formed plates. In the following sections, both the overall curvature and local geometric deviation along cross sections A-A and B-B will be analyzed.

4 Results and discussion

To verify the feasibility of forming higher accuracy spherical surface and investigate the forming mechanism in DS-MPF process, both the experiment and simulation with the optimized toolpath 3 were conducted. Analysis of results focused on geometric comparison, thickness distribution, strain analysis (especially the distribution and the evolutionary process of the bending strain), and forming force history.

4.1 Geometric analysis

With toolpath 3, the forming had been conducted using the equipment described in Sec. 3.1. Fig. 15 a presents the outer surface of the formed plate. Generally, a large forming force in the center causes an obvious bulge. However, closely spaced

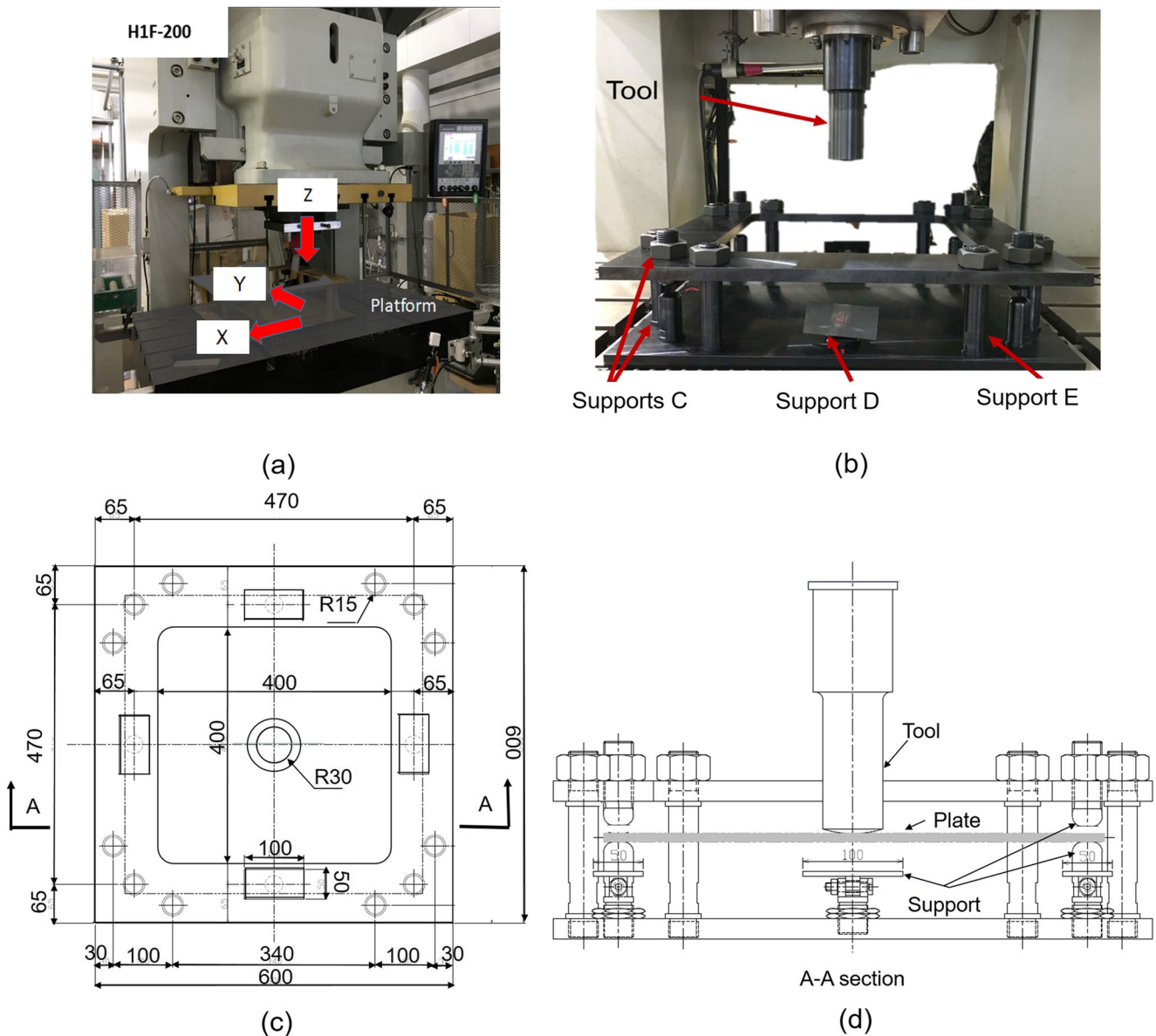


Fig. 13 (a) The experiment setup and (b) the designed tool and jig from (c) top view and (d) A-A section view

strokes around the center in toolpath 3 changed the formed profile by toolpath 1 to be smooth. The profile comparison along sections A-A and B-B in Fig. 15b and c shows a good agreement between experimental and simulated results. Also, the formed plate had a small local deviation as compared with the target. It indicates the feasibility of the DS-MPF forming method, and its toolpath design principle has been verified. Fig. 15 d and e present profile comparison between toolpath 1, toolpath 3, and the target. Radii of curvature along sections A-A and B-B with toolpath 3 were 984 mm and 1057 mm, respectively. For A-A and B-B, the maximum deviation by toolpath 3 decreased from 6.7 to 3.5 mm. No obvious deviation occurred in the central area. The dimple caused by the first stroke in toolpath 1 was much diminished by the added strokes close to the central region.

In toolpath 3, 24 strokes were added based on toolpath 1, thus creating reasonably closely spaced strokes. For part formed by toolpath 3, the Z-displacements of several points in Fig. 16a from inside to outside were recorded in Fig. 16b. The plate had spring back after each stroke; the degree of spring back depended on the size of the forming distance in the Z direction. As the number of strokes increased, the Z directional motion was rapidly reduced. When enough strokes were conducted in the outer areas, Z directional motion in the inner area was limited, tending to be a local forming process. After finishing the first point 27 in the 4th loop, the following points 29, 31, and 33 in the same loop had small spring back and then returned to their initial position; Z-displacements of points 1 and 18 in inner loops were also small. As a result, the DS-MPF forming tends to be a local forming method, which

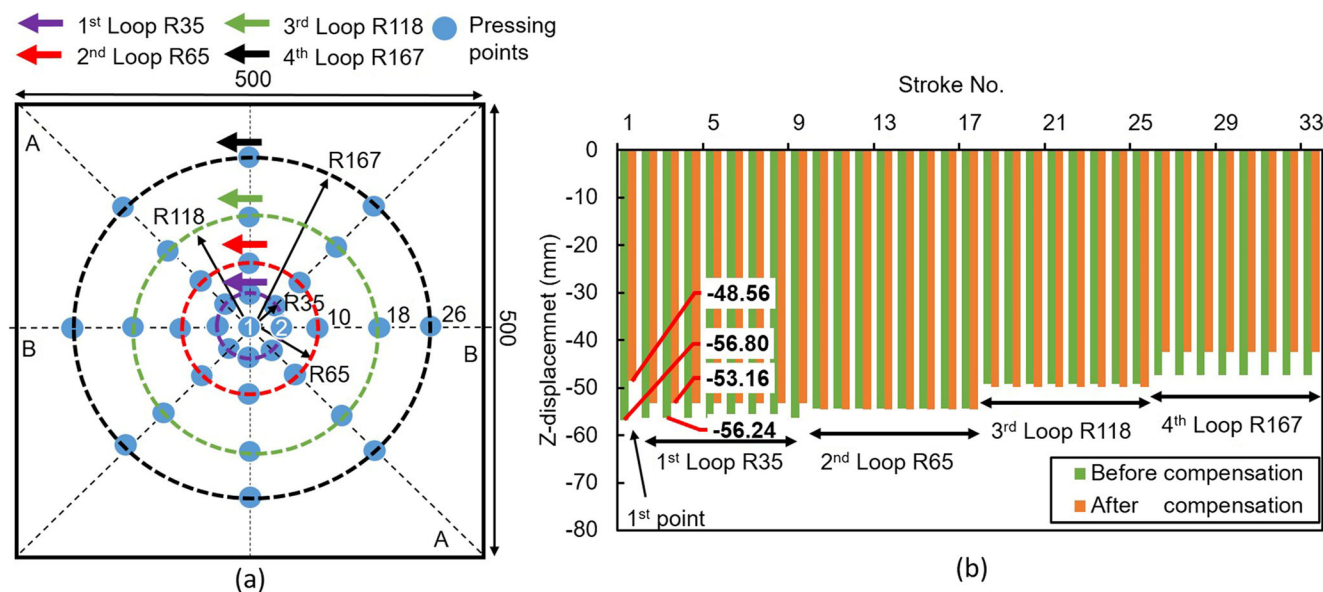


Fig. 14 Toolpath 3 with (a) position of 33 strokes, (b) Z-displacement of each stroke before compensation and after compensation

implies that the Z-displacement deviation in each loop can be corrected by the toolpath compensation method without causing significant Z-displacement in other regions.

To examine the influence of the forming sequence, simulated plates formed with IN/OUT (toolpath 3) and OUT/IN (reverse forming sequence based on toolpath 3) toolpaths

Fig. 15 (a) Outer surface of the formed plate. Profile comparison between simulated and experimental results with toolpath 3, and target along sections (b) A-A and (c) B-B. Profile comparison between simulated parts by toolpath 1 and 3, and the target along sections (d) A-A and (e) B-B

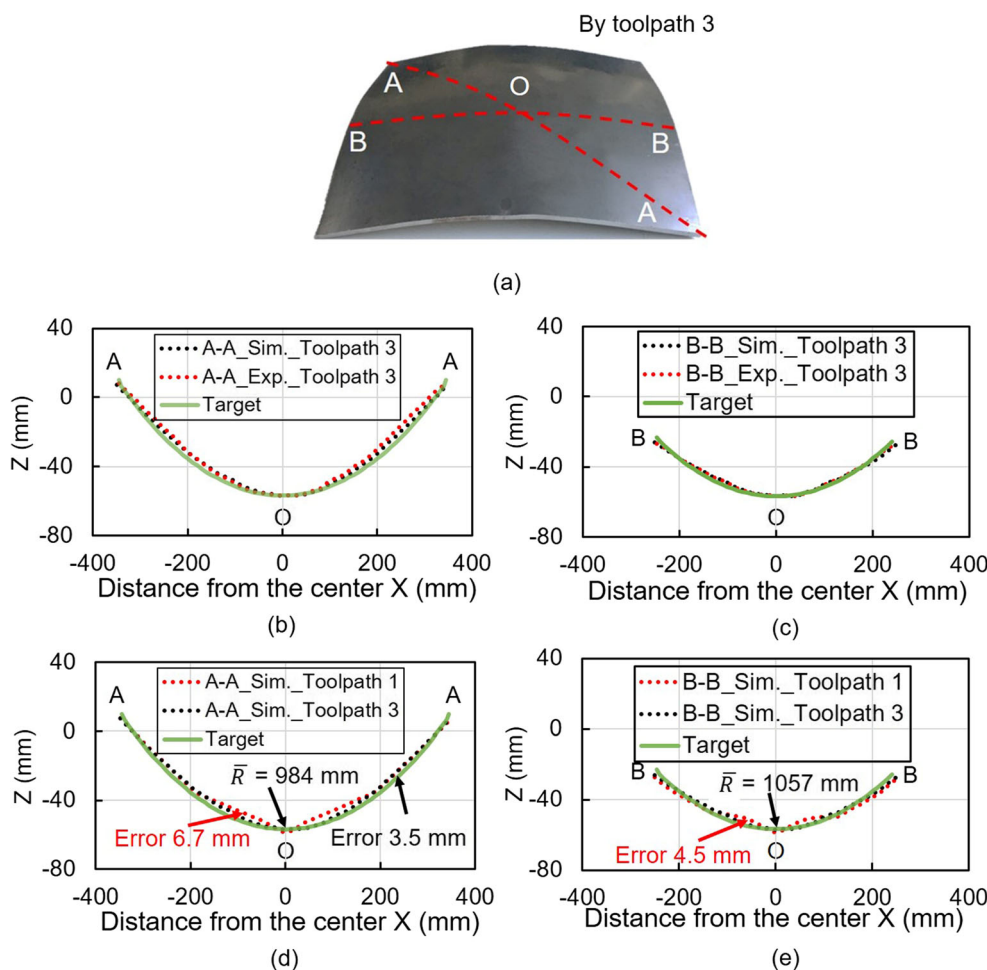
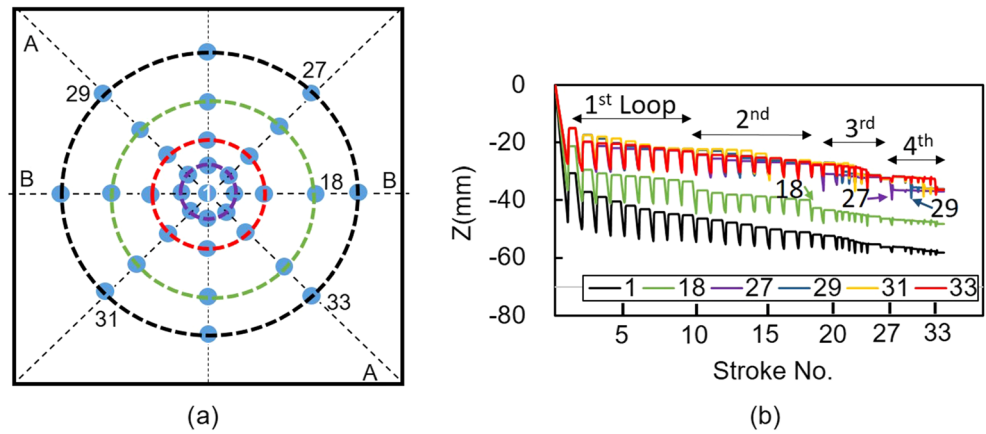


Fig. 16 (a) Selected points in toolpath 3 and (b) their Z-displacement history



were plotted in Fig. 17a and b. Compared to Fig. 17a, the maximum Z-displacement in Fig. 17b was -52.32 mm, which was further away from the target value of -56.8 mm; meanwhile, the edges of zone A were less smooth, and the center of zone B was flatter.

The relative overall radii of curvature errors δ were calculated from simulated profiles by different toolpaths along sections A-A and B-B (see Eq. (4)) and listed in Fig. 18. Values of δ along section A-A were -2.2% , 0.6% , and -1.6% ; for section B-B, the values of δ were 6.2% , 11.8% and 5.7% , respectively. It indicates that the IN/OUT toolpath can decrease a small relative error below 6% . Profile along section A-A had a lower value of δ as compared to section B-B.

4.2 Thickness distribution

Fig. 19 a shows one-half of the formed part with toolpath 3. No significant thinning occurred along the section, especially in the central region. After the formed plate was cut along sections A-A and B-B. The thickness values along sections OA and OB were measured at 10-mm intervals and compared with the simulated thickness values as shown in Fig. 19b. The thickness distributions along sections OA and OB were basically similar, with obvious wave-shaped thickness thinning at the same positions. Each wave trough referred to the positions of local bending points. The same thickness distributions

along different cross sections indicated that the formed parts in the DS-MPF process had good stability and rigidity. The minimum thickness value was 7.6 mm in the center area. The fluctuations of the outer layer thickness may be attributed to a slight rotation of the forming plate during the forming process or to deviations in the radius of curvature at the outer layer. The latter can be further altered by changing the stroke depth at each position to change the curvature and achieve a more uniform thickness distribution. The experimental and simulation results also matched well, indicating that the numerical model can be used to accurately predict the DS-MPF process.

4.3 Strain analysis

Fig. 20 presents the bending strain distribution history along the cross sections of the simulated formed parts. After the 1st point, the bending strain varied from the maximum value of 0.08 at area A to a negative value of -0.01 ; and then it continued rising and getting close to 0 from 25 to 100 mm. High bending strain about 0.08 at area A and wide contact area with the size of 50 mm (area for the tensile strain caused by the first stroke) improve the overall stiffness for further strokes; thus further strokes far away from the center may not change the original bending strain distribution and overall shape. However, a large bending strain caused a large deflection, and additional strokes on the 1st loop with R equal to

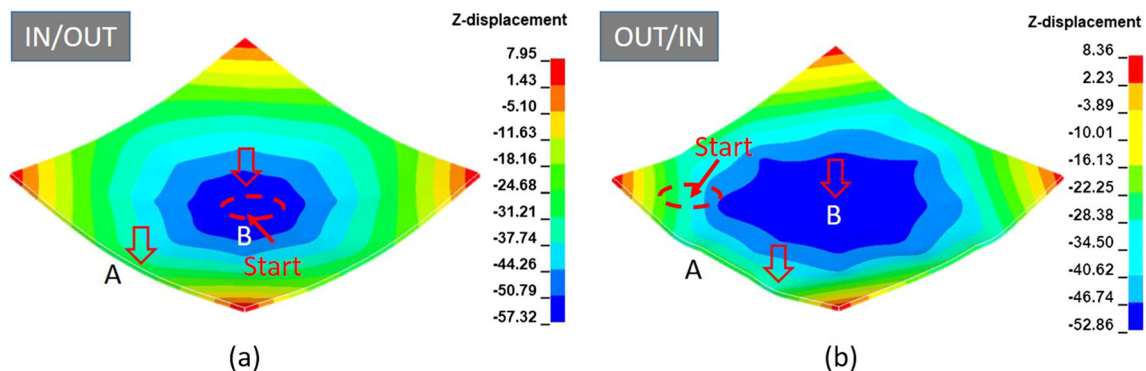


Fig. 17 Geometric comparison between formed parts with (a) IN/OUT and (b) OUT/IN toolpath

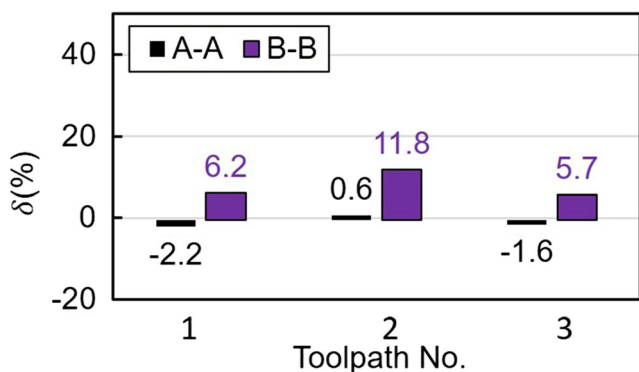


Fig. 18 Error δ comparison of simulated profiles along sections A-A and B-B

35 mm were needed to apply close to the 1st point to bring down the initial bending strain from 0.08 to 0.05. Two crests both had peak values close to 0.06. The minimum negative bending strain value had a bit drop from -0.01 to -0.02 . Further, after the 2nd loop with R65 mm, the three waves occurred with peak values close to 0.06. For the 2nd loop with R65 mm, the predicted R_C from Eq. (7) was 72 mm, close to the center of the third crest ($R_C = 80$ mm). Only a slight change in bending strain occurred at the uncontacted area. It implied that effects of strokes far away from the center on the bending strain of the central area were limited and decreases as R rises. As the width of bending strain wave decreases from 30 to 20 mm, the forming force will gradually diminish from inside to outside.

To explain how deflection (positive bending strain) under the tool and bulge (negative bending strain) between adjacent strokes occurs, Fig. 21 a presents a schematic of a contact area between the tool and a formed plate in the process of the 1st point stroke. Tool moved from 0 to 48.6 mm in Z direction. The strain distribution on the upper and lower surface was plotted in Fig. 21b. As Z changed from 10 to 48 mm, for area A, the strain on the lower surface had a tensile strain, rising from 0.003 to 0.059; the strain on the upper surface had a small compression strain, varying from -0.004 to -0.024 . For periphery area B, when Z increased from 30 to 48 mm, tensile strain occurred on the upper surface, varying from 0.000 to 0.005. In the forming process, the positive bending

Fig. 19 (a) The B-B section view of the formed plate with toolpath 3 and (b) the measured and simulated thickness distribution along sections A-A and B-B

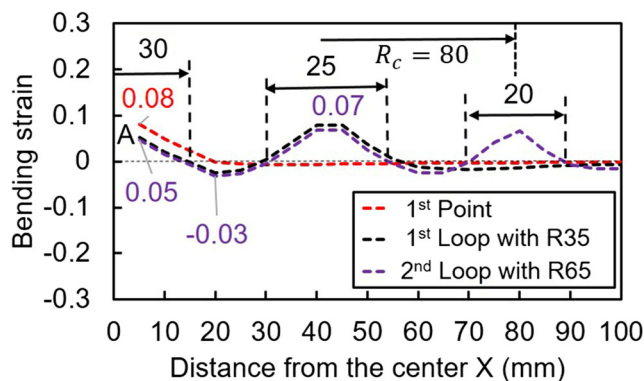
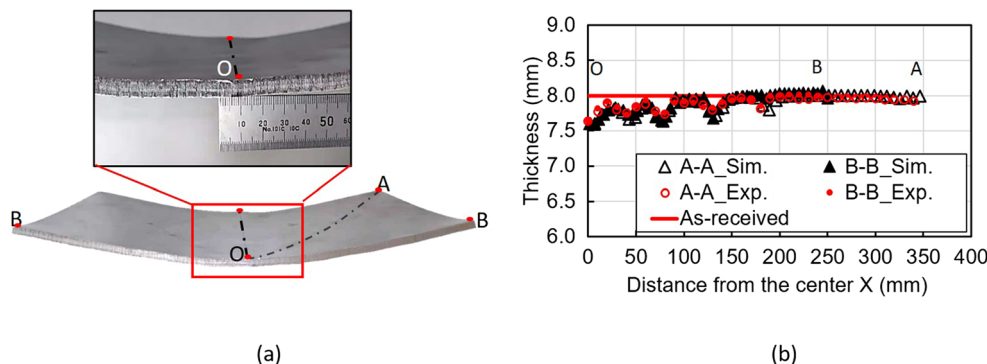
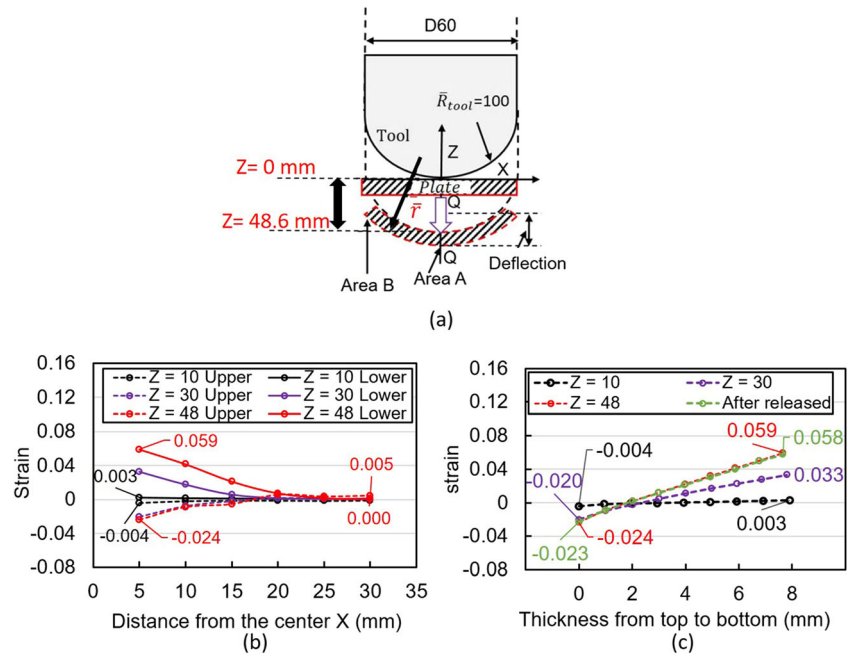


Fig. 20 Bending strain distribution $\Delta\epsilon_x$ bending comparison between the simulated formed plates after the 1st point, after the 1st Loop, and after the 2nd loop

strain was kept rising. When it arrived at a very large depth, the tensile strain on the upper surface turned to be positive and induced a bulge with negative bending strain at the tool-uncontacted area between adjacent strokes. Fig. 21 c displays the train history of the central area A along the thickness direction. Strain during the 1st stroke was recorded when Z equals 10, 30, 48, and 48.6 mm (after the tool was released). The neutral plane moved closer to the upper surface. The strain on the upper surface decreased from -0.004 to -0.023 . The strain on the lower surface kept rising from 0.003 to 0.058. The membrane tensile strain kept increasing during the 1st stroke; however, the final value was small, below 0.025.

The maximum Z-displacement change of plate at the peripheral area B in Fig. 21a was named as the deflection. Its value was related to the bending strain and the local radius of curvature \bar{r} under the tool. According to the simulated result in the first two loops, the strain distribution history of the central area A in Fig. 21a was drawn along the thickness direction. Fig. 22 b shows the corresponding local radius of curvature \bar{r} and its formed deflection of the central area B after each loop. In Fig. 22a, the strain on the upper surface rose from -0.023 to 0.001 in the forming process; the strain on the lower surface had a decline from 0.058 to 0.047. In Fig. 22b, correspondingly, the local radius of curvature of the central point

Fig. 21 The simulated result in the 1st stroke. (a) The schematic diagram of 1st stroke for the central point Q (Z changes from 0 to 48.6 mm) of the plate. (b) The strain history along X direction (areas A and B) and (c) along the thickness direction at area A.



increased from 194 to 453 mm and then to 765 mm; the formed deflection dropped from 2.35 to 1.0 mm and finally to 0.59 mm, close to the target deflection of 0.45 mm corresponding to the radius of curvature equal to 1000 mm.

4.4 Forming force analysis

In DS-MPF process with toolpath 3, the simulated forming force with simple supports was much smaller than that with fixed boundary near each support C due to the reduced membrane stress. During the 1st stroke, the forming force with simple supports increased to 69 kN with a lower slope in comparison to that with the fixed boundary (Fig. 23a). For the whole forming process with toolpath 3, the vertical peak forces of each stroke are also plotted in Fig. 23b. The maximum vertical peak force was about 90 kN. From the 1st loop to the 4th loop, peak forming force tended to decrease due to this width reduction of the bending strain wave in Fig. 20.

4.5 Future work

As a new technology for forming 3D curved thick plate, a series of significant advantages of DS-MPF should be clarified: no die investment, high flexibility, and high efficiency due to freely changeable strokes routes and the limited number of strokes, suitable for very thick plates, no thickness reduction and forming size limitation because of arbitrarily placed supports. However, there are still some forming issues needed to be optimized in the future, including dent marks on the inner surface, a slight rotation during the forming process, forming accuracy especially the edge area affected by the forming sequence and boundary condition. Based on the above issues, different boundary conditions, tooltip radius, and the thickness value of thin sheets will also be investigated to improve the forming accuracy of a formed part and to expand the application of DS-MPF.

Fig. 22 The simulated result in the first two loops. (a) Strain distribution at area A and (b) local radius of curvature \bar{r} and formed deflection at area B.

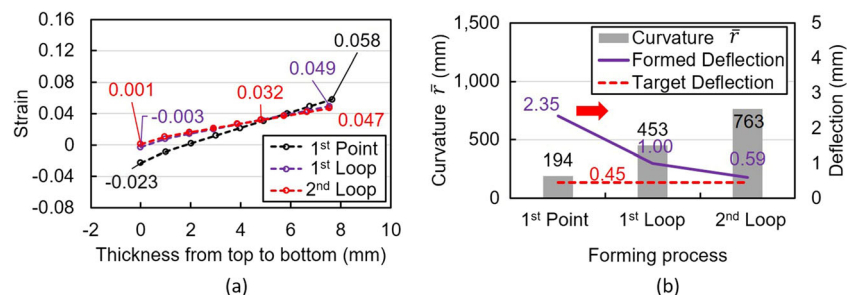
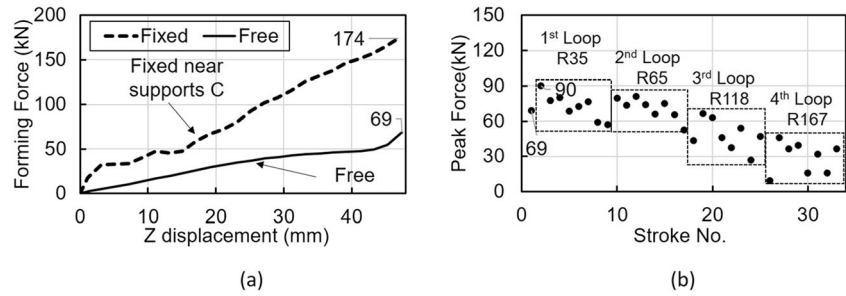


Fig. 23 (a) Simulated forming force in the 1st stroke with a fixed boundary and simple support boundary in DS-MPF. (b) Peak forming force of each stroke with toolpath 3



5 Conclusions

New DS-MPF technology has been developed which shows great potential and high efficiency in the forming of not-very-thin plates. A numerical model and experiment setup were established and manufactured to successfully form the target shape. The whole process can easily be transferred to be automatic and finished with several strokes.

From the geometric and thickness distribution analysis, it was figured out that the mechanism of DS-MPF belongs to local bending forming. The toolpath design principle of DS-MPF for a spherical surface is based on the concept of controlling the local bending strain at each stroke (adjusting their deflections) and changing stroke distribution.

For achieving a curved plate with a simple tool, the allowable process window regarding the maximum distance R and the maximum geometric error ΔH can be derived by a fitting formula. For the 8 mm SS400 plate with a radius of curvature of 1000 mm, the maximum bending strain was close to 0.06 at each stroke. Keeping adjacent strokes within a distance of 100 mm can reduce the profile error below 4.00 mm. Using this optimized toolpath according to the above-mentioned principle made the formed part smooth and with high overall and local profile accuracy.

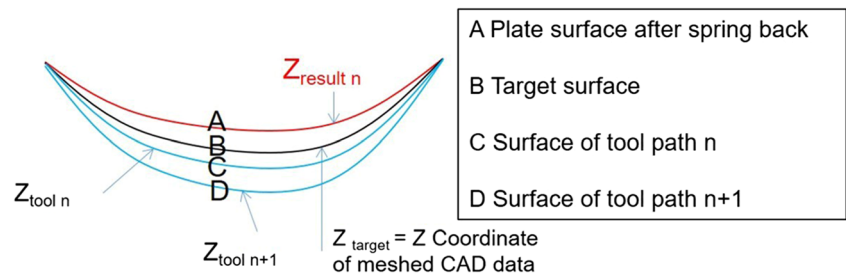
Using a forming sequence IN/OUT, a large peak value of bending strain and a wide area of bending strain distribution caused by the first stroke would make the formed part had a better profile accuracy compared with that with a sequence of OUT/IN. IN/OUT toolpath can achieve plates with small relative radii of curvature error below 6%. As the width of the bending strain area gets smaller, the peak forming force for 8-mm-thick

plate forming decreases rapidly; the peak forming force with free boundary is much smaller than that with a fixed boundary.

Appendix. Toolpath compensation for spring back

Due to the elastic strain component $\epsilon_{elastic}$, spring back of plate after each stroke will lead to some deviation from the target. Modifying the toolpath to compensate for this deviation is needed. All strokes in this toolpath are kept at the same position X and Y. Only Z coordinates are adjusted. Since the behavior is non-linear, compensation is carried out by iteration in several steps. The result of each iteration step, by analysis or physical testing, is used to find out the stroke Z of the next step, until the resulting surface converges to the target surface within the allowable tolerances. The strokes Z of the last iteration is to be used in forming. Fig. 24 shows a cross section of four surfaces used in compensation calculations: (A) plate surface after spring back, (B) the surface of the target, (C) surface used to calculate Z coordinates of the toolpath in the last iteration cycle n, and (D) surface to be used to calculate Z coordinates of the toolpath in the next iteration cycle n+1. Z coordinate of each point on surface D is calculated as given by Eq. (12). The logic behind this equation is that if a toolpath calculated using surface C produces surface A, then a toolpath calculated using surface D, as corrected by Eq. 12, should produce surface B.

Fig. 24 A-1 Compensation logic of Z-displacement along the cross-section



$$Z_{tool\ n+1} = Z_{tool\ n} + (Z_{target} - Z_{result\ n}) \tag{12}$$

Availability of data and material All data generated or analyzed during the present study are included in this published article.

Code availability Not applicable

Author contribution Song Wu: Methodology, equipment design, completion of experiment and simulation, and paper writing. Ninshu Ma: Conceptualization, modification, project management, and funding acquisition. Sherif Rashed: Manuscript modification and language proofing. Naoki Osawa: Modification. Thanks for the assistance in experiment provided by Mr. Matsuoka (Yusuke Matsuoka) from Osaka University.

Funding This work is supported by the Amada Foundation (AF-2018010: R&D of Die-less Incremental Plate Forming).

Declarations

Ethics approval Not applicable

Consent to participate Not applicable

Consent for publication Not applicable

Competing interests The authors declare no competing interests.

References

1. Das B, Biswas P (2018) A review of plate forming by line heating. *J Ship Product Des* 34(2):155–167
2. Li M, Liu Y, Su S, Li G (1999) Multi-point forming: a flexible manufacturing method for a 3-d surface sheet. *J Mater Process Technol* 87(1-3):277–280
3. Heo SC, Seo YH, Ku TW, Kang BS (2010) A study on thick plate forming using flexible forming process and its application to a simply curved plate. *Int J Adv Manuf Technol* 51(1-4):103–115
4. Shen W, Yan RJ, Lin Y, Fu HQ (2018) Residual stress analysis of hull plate in multi-point forming. *J Constr Steel Res* 148:65–76
5. Zhongyi C, Mingzhe L (2001) Optimum path forming technique for sheet metal and its realization in multi-point forming. *J Mater Process Technol* 110(2):136–141
6. Jia BB, Wang WW (2017) New process of multi-point forming with individually controlled force-displacement and mechanism of inhibiting springback. *Int J Adv Manuf Technol* 90(9):3801–3810
7. Dang X, He K, Li W, Zuo Q, Du R (2017) Incremental bending of three-dimensional free form metal plates using minimum energy principle and model-less control. *J Manuf Sci Eng* 139(7)
8. Li Y, Shi Z, Rong Q, Zhou W, Lin J (2019) Effect of pin arrangement on formed shape with sparse multi-point flexible tool for creep age forming. *Int J Mach Tools Manuf* 140:48–61
9. Silva MB, Skjødt M, Martins PA, Bay N (2008) Revisiting the fundamentals of single point incremental forming by means of membrane analysis. *Int J Mach Tools Manuf* 48(1):73–83
10. Young D, Jeswiet J (2004) Wall thickness variations in single-point incremental forming. *Proc Inst Mech Eng B J Eng Manuf* 218(11):1453–1459
11. Behera AK, de Sousa RA, Ingarao G, Oleksik V (2017) Single point incremental forming: an assessment of the progress and technology trends from 2005 to 2015. *J Manuf Process* 27:37–62
12. Tiesheng Z, Zhensheng L, Changji G, Zheng T (1992) Explosive forming of spherical metal vessels without dies. *J Mater Process Technol* 31(1-2):135–145
13. Zhang R, Iyama H, Fujita M, Zhang TS (1999) Optimum structure design method for non-die explosive forming of spherical vessel technology. *J Mater Process Technol* 85(1-3):217–219
14. Mehrasa H, Liaghat G, Javabvar D (2012) Experimental analysis and simulation of effective factors on explosive forming of spherical vessel using prefabricated four cones vessel structures. *Open Eng* 2(4):656–664

Publisher's note Springer Nature remains neutral with regard to jurisdictional claims in published maps and institutional affiliations.